

Techniques for reducing fiber-fed and integral-field spectroscopy data

The software package R3D

S.F.Sánchez,*¹

Centro Astronómico Hispano Alemán, Calar Alto, CSIC-MPG, C/Jesús Durbán Remón 2-2, E-04004 Almería, Spain

The dates of receipt and acceptance should be inserted later

This paper describes the general characteristics of raw data from fiber-fed spectrographs in general and fiber-fed IFUs in particular. The different steps of the data reduction are presented, and the techniques used to address the unusual characteristics of these data are described in detail. These techniques have been implemented in a specialized software package, R3D, developed to reduce fiber-based integral field spectroscopy (IFS) data. The package comprises a set of command-line routines adapted for each of these steps, suitable for creating pipelines. The routines have been tested against simulations, and against real data from various integral field spectrographs (PMAS, PPAK, GMOS, VIMOS and INTEGRAL). Particular attention is paid to the treatment of cross-talk.

© 0000 WILEY-VCH Verlag GmbH & Co. KGaA, Weinheim

1 Introduction

In fiber-fed spectrographs the slit is not placed at the focal plane of the telescope. Instead, the light from different locations on the sky is conducted into the spectrograph using optical fibers. At one end, the optical fibers are located in the focal plane of the telescope and at the other they are rearranged along the slit of the spectrograph, in the so-called pseudo-slit. Fiber-fed spectrographs are normally used for multi-object spectroscopy (MOS), where the fiber ends in the focal plane of the telescope can be placed at different positions on the sky, or for Integral Field Spectroscopy (IFS), where the fibers are packed in bundles or coupled with arrays of lenses.

Integral Field Spectroscopy (IFS) is a technique for obtaining multiple spectra simultaneously of a (more or less) contiguous area of the sky. Although fiber-fed spectrographs are widely used, there are other techniques to conduct the light from different positions in the sky to the spectrograph, e.g. lens arrays and image slicers. These different implementations have produced a set of instruments, which, while sharing the basics of the technique, produce very different representations of the spectra at the detectors. This apparent diversity has led to the development of reduction techniques and/or packages for each individual instrument (e.g., P3d, Becker 2001; Roth et al. 2005; VIPGI, Scodeggio et al. 2005; GEMINI, Turner et al. 2006). Together with the inherent complexity of this technique, this has reduced the use of IFS for decades to a handful of specialists, each usually working with a specific instrument.

IFS developers became aware of this handicap, and have started to produce standard techniques and tools valid for

any integral field unit (IFU). In a recent effort, the Euro3D RTN (Walsh & Roth 2002) has created a standard data format (Kissler-Patig et al. 2004), a coding platform (Pécontal-Rousset et al. 2004) and a visualization tool (Sánchez 2004), useful for any of the existing IFU. All these tools are freely distributed to the community. However most of them are for working with reduced data, while the reduction itself has still not been addressed with a generalistic approach. The astronomical community is confronted with a jungle of different instrument-specific pipelines, whose procedures and parameters differ greatly, and whose outputs are difficult to compare. Building on earlier work, we present here a summary of the most important steps in the reduction of data from fiber-fed spectrographs in general, and fiber-fed IFS in particular. All of them have been implemented in R3D, a reduction package able to reduce data from any fiber-fed IFU, whose main characteristics we also present.

The structure of this article is as follows. Section 2 describes the coding platform used to develop R3D. Section 3 summarizes the major characteristics of the raw data from fiber-fed spectrographs. The different steps required for a proper data reduction are explained in Section 4. In Section 5 we compare R3D with other packages in existence. Section 6 summarizes the conclusions. The data examples shown throughout this article are from PMAS (Roth et al. 2005) in the PPAK mode (Kelz et al. 2006), using 2×2 pixel binning, although R3D is not limited to this instrument/setup. For examples of its use with another instruments, please consult Sánchez & Cardiel (2005).

* Based on observations collected at the Centro Astronómico Hispano Alemán (CAHA) at Calar Alto, operated jointly by the Max-Planck Institut für Astronomie and the Instituto de Astrofísica de Andalucía (CSIC)

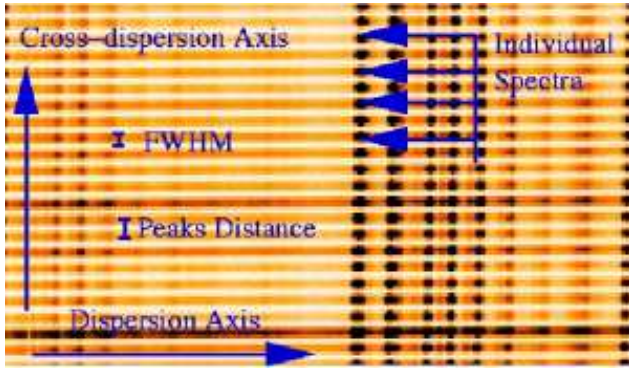


Fig. 1 Grayscale of a section of IFS raw data corresponding to PMAS in the PPAK mode, in inverse colors (i.e., more intense areas are shown in darker colors). Each dark line corresponds to the projection of a spectrum along the dispersion axis (indicated with an arrow), which in this case corresponds to the X-axis. Spectra are separated ~ 5 pixels across the Y-axis, the cross-dispersion axis, and projected in following a pseudo-Gaussian of $\text{FWHM} \sim 3$ pixels, contaminating the adjacent spectra.

2 Coding platform

We first coded the algorithms in `perl`, using the Perl data language¹, in order to speed-up the algorithm testing phase. Once we tested the algorithms with simulated and real data, we recoded the most time consuming ones in C to increase their performance. The `perl` version of R3D is fast enough to produce valuable science frames in a reasonable time, although for instruments with many fibers (like VIMOS, LeFevre et al. 2003), or for some slow processes like cross-talk correction algorithms, we strongly recommend the C-version. Both versions use `PGPLOT` as graphical library (Pearson 1995), and the C version uses the Lyon-C-Library and the Euro3D development environment (Pécontal-Rousset et al. 2004). A major advantage of using `perl` and C is that they are freely distributed, platform independent, languages, and therefore R3D can be installed under almost any architecture without major effort and at no cost. R3D has been coded as a package of independent command-line routines, and therefore it is possible to create pipelines and super-scripts that run the same sequence of commands over different input data. This ensures the homogeneity and repeatability of the data reduction process. Download and installation instructions for R3D are available via its webpage².

3 The raw data of fiber-fed spectrographs

In most cases, the raw data of fiber-fed spectrographs consist of a collection of spectra distributed along a certain axis of a 2D frame. Figure 1 shows an example of IFS raw data, corresponding to PMAS (Roth et al. 2005) in the PPAK

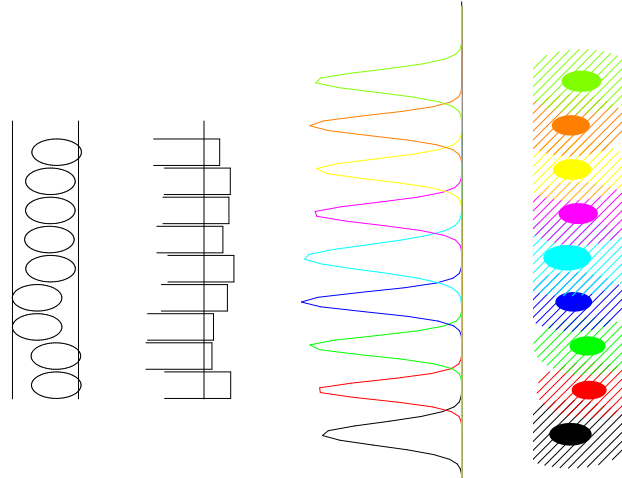


Fig. 2 The left panel shows two sketches of the distribution of the fibers in the plane of the pseudo-slit, as viewed from both the front and the side. Both projections show the misalignments of the fibers. The right panel shows a scheme of the spectra projected in the CCD plane. It presents an intensity cut along the cross-dispersion. The intensity profile of each spectrum is shown a different color, illustrating the cross-talk effect. The spots simulate emission lines as they are seen in the raw data (see 1), with 1σ cut represented as solid and 3σ as hashed ellipses. They illustrate the effects of the misalignment on the dispersion.

mode (Kelz et al. 2006), illustrating this distribution. Each spectrum is distributed in one direction with wavelength, along the so-called dispersion axis. For each wavelength, it is also spread along the perpendicular or “cross-dispersion” (or “spatial”) axis, following a characteristic profile of finite width, which may be considered Gaussian in the simplest approximation. If the spectra are tightly packed, contamination occurs among neighbors. This is referred to as cross-talk (see Fig. 1). Due to the mapping of the fibers, adjacent spectra at the CCD may originate from distant locations in the sky plane. The cross-dispersion profile varies with position along the pseudo-slit, generally being more symmetrical in the center. The profile also varies along the dispersion axis (e.g., Becker et al. 2000; Becker 2001). Spectrographs are generally designed to minimize the effects of cross-talk (e.g., Bershadsky et al. 2004). However, there is always a trade-off between the number of fibers “packed” in the spectrograph, the size of the CCD and the width of the profiles, and the final cross-talk. In addition, the spectra are never perfectly aligned along the dispersion axis due to the configuration of the instrument, its setup, the instrument focus, and any flexure effects. The transmission also changes fiber-to-fiber due to different tensions, slight misalignments, and intrinsic physical differences. These imperfections also affect the width of the projected profiles along both the cross-dispersion and the dispersion axes, and introduce small differences in the spectral dispersion from fiber to fiber.

¹ <http://pdl.perl.org>

² <http://www.caha.es/sanchez/r3d/>

Figure 2 illustrates all these effects. The left panel shows a sketch of the distribution of the fibers in the plane of the pseudo-slit, as viewed from both the front and the side. Due to the misalignments of the fibers with respect to the axis of the pseudo slit, the light coming from each fiber enters the spectrograph with small offsets relative to one another. Therefore, the dispersion solution varies slightly from fiber to fiber. Meanwhile, the offsets with respect to the focal plane produce differences in the profiles of the projected spectra at the CCD, as described before. The right panel shows these projections in the CCD plane. It presents an intensity cut along the cross-dispersion, where the intensity profile of each spectrum is shown a different color. It illustrates the cross-talk, the variations in focus, and the fiber-to-fiber transmission. The spots simulate an emission line as seen in the raw data, illustrating the differences in the dispersion solution. The same effect can be seen directly in the raw data (Fig. 1).

In any spectrograph, the spectral resolution changes from the center of the slit to its edges. This is due to optical aberrations, which vary as a function of field angle and of wavelength. This well-known effect is further complicated by the differences among the fibers, as discussed above. The process of sky subtraction is particularly problematic, not only because adjacent spectra at the CCD may correspond to distant locations on the sky, but also due to the above-mentioned differences in the dispersion solution from fiber to fiber. All of these instrumental effects have to be addressed in the data reduction.

4 Procedures for the data reduction

All fiber-fed spectrographs yield similar raw data. Thus the data reduction process generally follows the same sequence of steps, regardless of the specific instrument involved. As a starting point for the reduction, it is assumed that the data have been bias and flat-field corrected (when possible), with an external tool. After these corrections, the data reduction consists of: (a) identification of the position of the spectra on the detector for each pixel along the dispersion axis, (b) scattered light subtraction and extraction of each individual spectrum, (c) distortion correction of the extracted spectra, and determination of the wavelength solution (i.e., dispersion correction), (d) correction of the differences in the fiber-to-fiber transmission, (e) flux calibration, and (f) sky emission subtraction. For IFUs it is also required to (g) re-order the spectra on their original location in the sky and (h) correct for the differential atmospheric refraction (DAR). Each of these reduction steps has been treated with a set of command-line routines in R3D. For clarity, we will assume hereafter that the dispersion axis is the X-axis and the cross-dispersion the Y-axis (although this is not a limitation of R3D).

4.1 Finding & tracing the position of the spectra on the raw frame

The location of the spectra is found at a certain column on the CCD by comparing the intensity at each row along the column (or a coadded set of columns around it) with that of n adjacent pixels, looking for those pixels that verify the maximum criteria, while requiring a minimum distance from the previous maximum. Let be i the pixel in the dispersion axis indicating the selected column in the CCD, the j -pixel is the location of the peak number k if it is the k th pixel that verifies:

$$I(i, j - n) < \dots < I(i, j - 1) < I(i, j) \text{ and} \\ I(i, j) > \dots > I(i, j + n - 1) > I(i, j + n)$$

and

$$|j_k - j_{k-1}| > \text{min_dist}$$

where min_dist is the minimum distance between adjacent maxima, and $I(i, j)$ is the intensity in the raw data at the (i, j) location.

Once the location of the peak intensity is determined at the resolution of one pixel, a more accurate centroid of that peak (y_{peak}) is determined with a simple parabolic maximum determination.

$$y_{\text{peak}} = (j + 1) - ([I(i, j + 1) - I(i, j)]/d + 0.5)$$

where

$$d = [I(i, j + 1) - 2I(i, j) + I(i, j - 1)]$$

The result is stored as an ASCII file, containing an identification number for each fiber/spectrum and the pixel and centroid position of the peak intensity. The process is cross-checked visually by a graphical output. Lost spectra, due to broken fibers or low contrast between adjacent pixels, or misidentifications due to cosmic rays can be handled by editing this ASCII file. It is also possible to refine the input parameters based on the visual inspection of the output to remove misclassified identifications and to increase the contrast. The input parameters to be modified are the minimum distance between adjacent pixels, the number of adjacent pixels to check for the maximum criteria, the number of columns in the dispersion axis to coadd to increase the signal-to-noise/contrast and the initial column to look for the peaks. E.g., cosmic-rays can be identified as peaks of a particular spectrum when the number of adjacent pixels used to identify the location of the peaks (n) is too low. Two possible solutions to this problem could be (i) to enlarge this number, forcing the procedure to identify not just a local maximum, but a profile, or (ii) to increase the width of coadded columns to blur the cosmic-rays.

The adopted procedure to identify the location of the spectra projected at a certain column of the CCD is independent of the pattern of the spectra spacing, i.e., if it is uniform/regular or not or if there are gaps in between different fibers. Indeed, it is not required to pre-define a certain pattern. However, a certain knowledge of this pattern (or the disposition of the fibers in the pseudo-slit) is required to visually discriminate between real spectra and misclassifications. Alternatively, one may use an external tool to create the ASCII file containing the location of the spectra on

the CCD at each column. This may then be cross-correlated with the real data and/or used as the input for the tracing routine. This option may be particularly appealing for instruments with many broken or low-transmission fibers like VIMOS.

Next, the tracing of the peak intensity along the dispersion axis is performed by looking for maxima around each original location within a certain window. The process is iterative, starting from the original column and continuing to the end of the CCD. If no maximum is found within the predefined window for a certain column, the location of the spectra on the previous column is used assuming a smooth behavior of the trace along the dispersion axis. This method solves the possible problems of bad columns, low sensitivity pixels, and/or cosmic rays. Again, the user may adjust the width of the input window, the number of adjacent pixels used to look for the maxima criteria, and the number of coadded columns to fine-tune the tracing procedure. The result is stored as a 2D image, where the X-axis corresponds to the original dispersion axis and the Y-axis indicates the traced spectrum number. The stored value at each pixel is the location of the peak centroid in the original frame of the given spectrum for each pixel in the spectral direction.

The tracing procedure must be applied over well illuminated continuum exposures. In many cases the science frames do not have enough signal-to-noise through all the fibers at any wavelength for an accurate determination of the tracing (e.g., emission-line dominated sources), and dome-flat exposures must be used (or similar ones). In the case of IFUs that suffer from flexures, these exposures may be taken immediately before and after the science exposures, and without moving the telescope from the position where the observations have been performed.

We tested the peak identification and tracing routines with simple simulated data, assuming Gaussian profiles with different FWHMs for the projection of the spectra along the cross-dispersion axis. The peak-to-peak separation was held constant. The location of the spectra at the CCD is recovered within 1 pixel whenever there is enough signal-to-noise per pixel (i.e., contrast between adjacent peaks). There is no typical value for the signal-to-noise to be considered good for the tracing procedure, since this process depends on other parameters, like the FWHM of the profiles along the cross-dispersion, the distance between adjacent spectra, the number of pixels compared for the maximum criteria, and the number of coadded columns.

4.2 Scattered light subtraction

Many spectrographs suffer from scattered light that contaminates the science and calibration exposures. This light comes from reflections in the instrument or light entering but not following the defined light-path. It is normally identified as a smooth background in-between the projected spectra on the raw data. It normally depends on the input illumination, and it has a greater effect on twilight sky exposures or long exposure time science frames in bright nights.

To correct for this, information between the projected spectra is required. Pixels affected by the projected spectra are masked out and the remaining background is interpolated to recover a map of the scattered light for the full frame. In R3D a scattered light map is obtained using the result from the tracing algorithm, masking the pixels of the input image within a defined aperture around the location of the spectra peaks for each pixel in the dispersion axis. Once masked, the remaining pixels are used to perform a polynomial function fitting along the cross-dispersion axis. The derived frame is then smoothed to estimate the scattered light map and subtracted from the input raw data.

The accuracy in the determination of the scattered light depends strongly on the fiber-packing, i.e., the way the fibers are ordered in the pseudo-slit. It is well determined if there is enough space in between fibers and/or the fibers are packed in groups with well defined separations. If the fibers are crowded, without *clean* spaces in between, and suffering from strong cross-talk contamination, it is almost unfeasible to estimate the scattered light.

4.3 Spectra extraction

After tracing the location of the spectra at the CCD, and subtracting the scattered-light (if needed), the next reduction step is to extract the flux corresponding to the different spectra at each pixel along the dispersion axis. The most simple method to perform this extraction is to coadd the flux within a certain aperture around the location of the spectra peaks in the raw data, using the tracing information, and storing the resulting spectra in a 2D image. This procedure is called aperture extraction, and it has been implemented in R3D. The X-axis of the resulting image corresponds to the original dispersion axis, while the Y-axis corresponds to the ordering of the spectra along the pseudo-slit. This is the so-called row-stacked spectra representation (RSS, Sánchez 2004). However, in most cases aperture extraction is not the optimal method to recover the flux corresponding to each spectrum. The distribution of the flux following pseudo-Gaussian profiles for each spectrum along the cross-dispersion axis limits the accuracy of the recovered spectra.

Figure 3, left panel, shows the percentage of flux recovered with an aperture extraction for different FWHMs of the profiles along the cross-dispersion axis (assuming Gaussian profiles) in units of the distance between adjacent spectra (Δ_{peaks} , also known as *spectral pitch*). The black dot-dashed line corresponds to a fixed aperture of the width of that distance, while the red solid-line corresponds to a growing aperture of 3 times the FWHM. In the first case there is an underestimation of the recovered flux, that grows with the FWHM of the profiles. This underestimation may be solved by enlarging the aperture, as shown in the second case. However, the contamination from flux coming from adjacent spectra (i.e., cross-talk) limits the size of the selected aperture. Figure 3, right panel, shows the percentage of flux of a given spectrum that is erroneously assigned to the nearest adjacent spectrum by an aperture extraction.

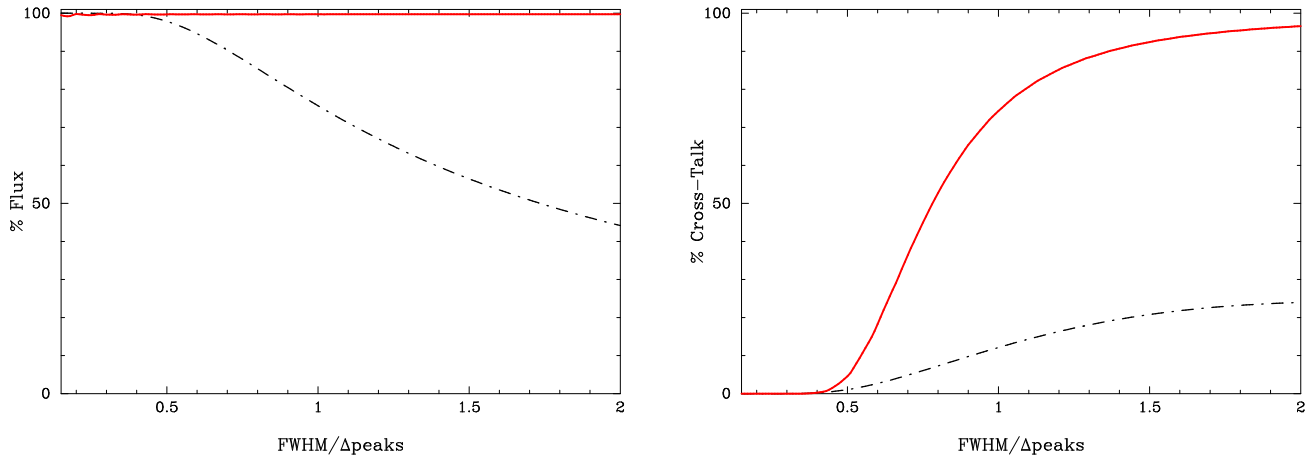


Fig. 3 Results from the simulations. Left-panel: Fraction of the input flux recovered by an aperture extraction of a set of simulated spectra plotted versus the ratio between the FWHM of the profiles along the cross-dispersion axis and the distance between the peak intensity of adjacent spectra ($\Delta peaks$). The two lines shows the results for two different apertures. The dot-dashed line shows the results for a fixed aperture of the distance between adjacent spectra. The solid-line shows the results for a variable aperture of 3 times the FWHM. Right-panel: Fraction of the input flux assigned by an aperture extraction to the adjacent one (i.e., the cross-talk) for the two different adopted apertures described above.

This percentage is plotted as a function of the FWHM of the instrumental profiles, where the two lines again correspond to the apertures described above. The cross-talk percentage grows with the FWHM for both aperture selections. It is important to note here that cross-talk is an incoherent contamination, and in many science cases and/or instrument designs it is preferable to keep it as low as possible: an average value of $\sim 1\%$ with a maximum of a $\sim 10\%$ (e.g., Bershadsky et al. 2004). For an aperture of $\sim \Delta peaks$, this level of cross-talk is found for $FWHMs \sim \Delta peaks$. However, in the case of an aperture that maximizes the recovered flux, the level of cross-talk is already $\sim 60\%$ for the same ratio between FWHMs and $\Delta peaks$.

The need for packing the largest possible number of spectra on CCDs with limited sizes ensures a certain level of cross talk. The FWHM of the projected profile along the cross-dispersion axis is normally defined by the design of the spectrograph and the size of the input fibers. Therefore, the ability to pack spectra with a reduced cross-talk is controlled by the ratio between these FWHMs and the defined $\Delta peaks$. A ratio of $FWHM \sim 0.5 \Delta peaks$ seems to be a good compromise for maximizing the packing of spectra at the CCD, without large cross-talk contamination. For illustration, PMAS/PPAK spectra profiles have a FWHM of the order of ~ 2.3 pixels, and a $\Delta peaks$ of ~ 5 pixels, in the 2×2 binning mode (Kelz et al. 2006). Selecting an aperture size of the order of $\Delta peaks$ seems to be an acceptable compromise between maximizing the recovered flux and minimizing the cross-talk, for aperture extractions. However, in some cases, when the raw frames are too crowded with spectra and the cross-talk is severe, this approach is not valid (e.g., Murray et al. 2000). On the other hand, there are spectrographs for which the $\Delta peaks$ is much larger than the FWHMs (e.g., PMAS in Larr mode, without nod&shuffle,

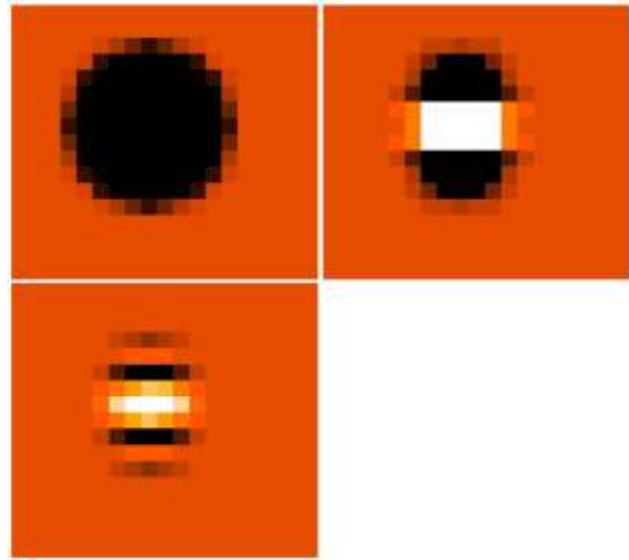


Fig. 5 Top-left: 20×20 spaxels intensity map of a simulated star with a Gaussian profile of 3 spaxels FWHM. Top-right: Result of the subtraction of the former map from the reconstructed map created after simulating a set of IFS data with the previous intensity distribution and reducing them using a pure aperture extraction. Bottom-left: Similar map obtained reducing the simulated data with a Gaussian-suppression extraction. The same grayscale range and scale intervals were used in the two latter panels.

Roth et al. 2005). In this case it is possible to maximize the fraction of recovered flux by enlarging the aperture, with a reduced cross-talk contamination.

The cross-talk may have strong implications in the interpretation of the data. In a general case, the adjacent spectra

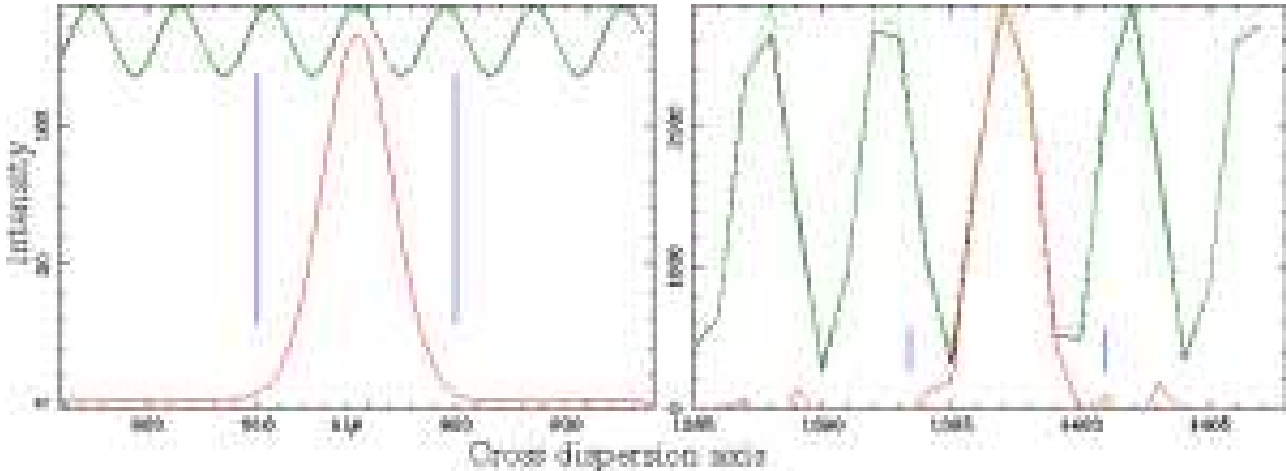


Fig. 4 Left-panel: Section of an intensity cut along the cross-dispersion of a simulated set of fiber-fed spectra (black solid-line), created assuming a Gaussian profile with a FWHM equal to the distance between adjacent fibers, i.e., a system with a strong cross-talk. No noise has been included in the simulation. The green dot-dashed line shows the modeled profiles created by the *Gaussian-suppression* technique, and the red solid-line indicates the recovered profile of the considered spectrum once decontaminated from the contribution of the adjacent spectra by this technique, assuming an initial aperture indicated by the vertical lines. Right-panel: Similar plot for real data of a continuum illuminated exposure obtained with the PPAK mode of the PMAS spectrograph, a system with a FWHM ~ 0.5 times the distance between adjacent fibers.

on the plane of the CCD may not correspond to nearby locations in the sky plane (e.g., PMAS and VIMOS). On the other hand, other instruments, like PMAS/PPAK and INTEGRAL (Arribas et al. 1998), have calibration-fibers located in between the science ones along the pseudo-slit. In both cases the cross-talk mix-up spectra from locations that may be not physically related or from spectra with a completely different nature.

Different techniques have been implemented to minimize the cross-talk. The full version of P3d (Becker 2001, Roth et al. 2005) uses an instrumental profile database to decouple the flux coming from adjacent spectra. This method is rather slow, and it has the disadvantage of requiring an accurate determination of the profiles. This is not always possible due to instrumental designs, and they may even change during the observing run. A more simple approach is to assume a Gaussian profile and perform a multi-Gaussian fit. We implemented this method in R3D, but it turned out to be too slow, and strongly dependent on the signal-to-noise of the data.

We developed a new technique that reduces the effects of the cross-talk and maximizes the recovered flux, named *Gaussian-suppression*. The technique works assuming that the spectral profiles are well approximated by Gaussian functions, and that the FWHMs of all of them are almost equal (this last assumption is not a limitation of the method, but a simplification). In a first iteration it performs an aperture extraction, as described above. Then for each spectrum the flux corresponding to n adjacent spectra is subtracted assuming a Gaussian function with the defined FWHM, and with the integrated intensity derived by previous aperture extraction (a multi-Gaussian approximation). Once the flux

from adjacent spectra is subtracted, a new aperture extraction is performed with the same or a different aperture.

Figure 4 illustrates the method. In the left panel, the solid black line shows a cut along the cross-dispersion axis for a simulated IFS raw frame created assuming Gaussian profiles for the projection of the spectra on the CCD, with a FWHM equal to the size of Δ_{peaks} (i.e., data with strong cross-talk). The green dashed-line shows the multi-Gaussian approximation, whose intensities are derived from the aperture extraction performed in the first iteration. The red solid-line shows the recovered profile after suppressing the flux coming from adjacent spectra. The method works well for severe spectral packing in the CCD. Figure 4, right panel, shows a similar plot for real data obtained with PMAS/PPAK. It illustrates the performance of the method in the presence of noise and for profiles without Gaussian shapes.

We strongly recommend the user to test the *Gaussian-suppression* technique with simulations that resemble as much as possible the science data before using it. The required input parameters are strongly dependent on: (1) the shape of the spectra projected along the cross-dispersion, (2) the distribution of the spectra at the CCD (e.g., homogeneously packed, packed in groups, or more or less randomly distributed), and (3) the position table of the fibers in the sky plane (i.e., if adjacent spectra at the CCD corresponds to adjacent positions in the sky). As a probe we simulated IFS data of a fiber-fed IFU with a lensarray of 20×20 spaxels, distributed in a regular grid with a square pattern (Fig 5). The spectra are projected along the cross-dispersion axis following Gaussian profiles of FWHM = 3.5 pixels, with a distance of 7 pixels between the peak emission of adjacent spectra. The simulated data is comprised of a model star with a Gaussian profile in the spatial direction with a

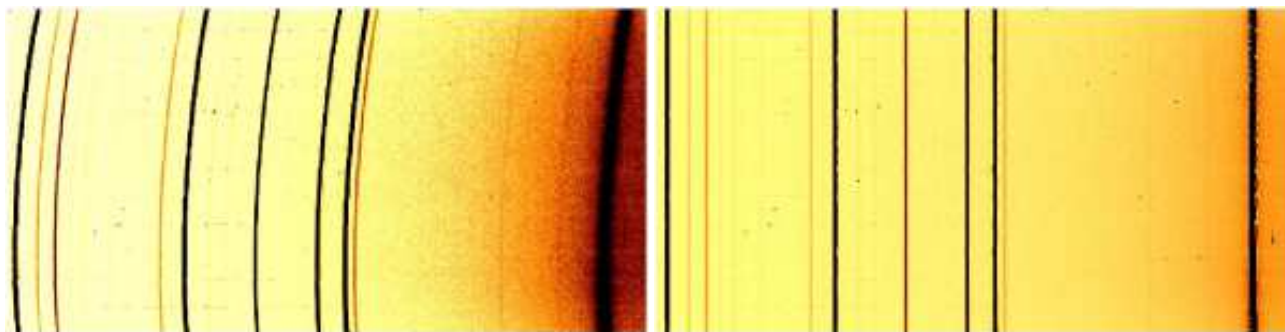


Fig. 6 Left panel: Example of extracted spectra of a calibration arc lamp obtained with PMAS in the PPAK mode. Right panel: Same data after wavelength calibration.

FWHM of 3 spaxels. No noise was included in this simulation. The simulated spectra are *reduced* using R3D, following the steps described above. The extraction was performed twice, using both a pure aperture extraction and the *Gaussian-suppression* technique. In the first case we used a 7 pixel aperture, following our previous results (Fig. 3). The flux is recovered within $\sim 10\%$ of the original values for any spaxel at any wavelength using an aperture extraction, and with a standard deviation of the residuals of $\sim 2\%$ of the original flux. In the second case we tested different combinations of parameters to recover as closely as possible the original integrated flux. We finally use an initial aperture of 6 pixels and a final one of 9 pixels. The original flux is recovered within $\sim 5\%$, with a standard deviation of the residuals of $\sim 0.5\%$.

Cross-talk between spectra, in combination with the mapping scheme of the spatial elements, causes distortions in the re-constructed images. In our simulated data the position table is sequential, from left-top to right-bottom, following the rectangular grid. In instruments with this kind of position table the re-constructed images are elongated (e.g., Roth et al. 2004). Figure 5 illustrates this effect. The top-left panel shows the input intensity map of the simulated star. The top-right panel shows the subtraction of this original map from the reconstructed map of the *reduced* data using a pure aperture extraction. As expected there is a transfer of flux from the peak emission along the vertical axis, that produces a flattening and elongation of the shape. The bottom-left panel shows a similar map for data *reduced* using the *Gaussian-suppression* extraction. The original shape is reconstructed better.

4.4 Distortion correction and wavelength solution

For grating spectrographs, the entrance slit is distorted and imaged as a curve onto the CCD (e.g., Meaburn et al. 1984). When fed with fibers, additional distortions are added to this intrinsic curvature due to the placing of the fibers in the pseudo-slit, as described in Section 3, Fig. 2. Figure 6, left panel, shows an example of extracted spectra where the curvature and distortions of the dispersion solution are seen. The data correspond to a calibration arc-lamp observed with

PMAS in the PPAK mode. The discontinuities and slight differences in the dispersion solution fiber-to-fiber prevent us from performing 2D modeling of the distortion map with an analytical function, nor at the level the extracted spectra, nor at that of the raw data. These *distortions* must be corrected fiber-to-fiber before finding a common wavelength solution.

R3D performs this correction in a two-step procedure, using arc calibration lamp exposures (like the one in Fig. 6). In the first step, the peak intensity of a single emission line is traced along the cross-dispersion axis, and shifted to a common reference, by a linear shift. After that, the intensity peak of a set of selected emission lines is traced, and a polynomial distortion correction is determined to recenter all the lines to a common reference. The distortion correction maps are stored to be applied subsequently to the science exposures. Figure 6, right panel, shows the same extracted spectra of the left panel after applying the distortion correction. A one dimensional spline interpolation algorithm is applied spectrum-to-spectrum in this process.

In the second step, the wavelength coordinate system is determined by identifying the wavelengths of the arc emission lines, using an interactive routine. The distortion-corrected spectra of the arcs are then transformed to a linear wavelength coordinate system by a one dimensional spline interpolation, assuming a polynomial transformation between both coordinate systems. The required transformation is stored in an ASCII file to be applied over the science data.

The accuracy of the final wavelength solution depends on the selected order of the polynomial function, the number of identified lines, and the coverage of emission lines along the wavelength range. These values depend strongly on the instrument and setup. For example, for PMAS in the PPAK mode, using the lowest resolution (e.g., V300 grating, Roth et al. 2005), it is possible to achieve an accuracy of $\sim 0.15\text{\AA}$ (*rms* of the fit) identifying just 9 emission lines and using a polynomial function of order 4. A similar accuracy is obtained for VIMOS in the High-resolution Orange mode by identifying 26 emission lines and using a polynomial function of order 5.

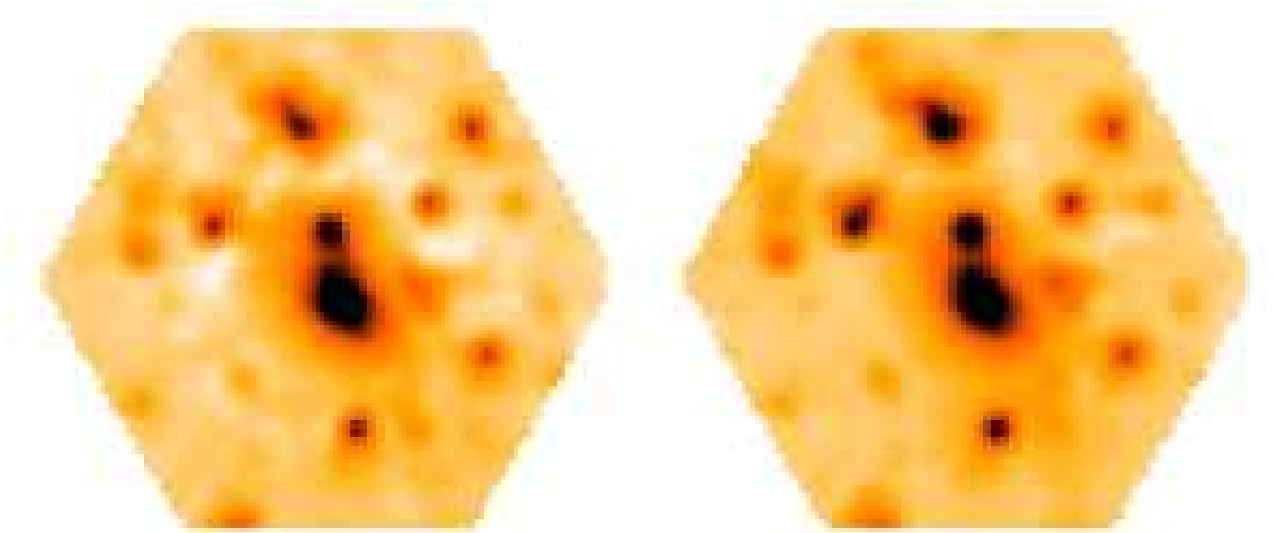


Fig. 7 Example of the effects of flat-fielding. The panels shows a map, extracted from a reduced and interpolated dataset of PPAK. Some structures seen in the left panel are artefacts that disappear after calibration of the differences in the fiber-to-fiber transmission.

4.5 Fiber-to-fiber response correction

For most IFUs, the transmission varies appreciably fiber-to-fiber. To correct for this, an exposure of a continuum, well-illuminated, and flat source is required, like a dome or sky flat. This exposure is used to determine the differences in the transmission fiber-to-fiber, by comparing the flux spectra-to-spectra, and deriving the so-called fiber-flat. In certain IFUs the fiber-flat shows a strong wavelength dependency, while in others this is unappreciable. R3D includes tools for deriving both kinds of fiber-flats. In the first case the spectra are divided by the median spectrum, obtaining a normalized fiber-flat, including the wavelength dependence. In the second case, the flux within a selected wavelength range is averaged for each spectrum and divided by the median of these values for all the spectra. In both cases, the science spectra must be divided by the obtained fiber-flat.

Figure 7 illustrates the importance of the fiber-flat correction. It shows a reconstructed map extracted from a datacube of PPAK data of the core of the galaxy cluster Abell 2218 (Sánchez et al. 2006), centered at $\sim 5780\text{\AA}$. The spectra were reduced with R3D, and rearranged in their spatial distribution and interpolated to create a regular grid datacube using E3D (Sánchez 2004), as discussed below. Left and right panels show the map before and after correcting for the differences in the fiber-to-fiber transmission. Note that before the correction, the image has an artificial ring-like structure, which is almost completely removed in the right panel. This is obviously seeing in IFS reconstructed maps, but it is difficult to identify in MOS spectroscopy. In both cases, the result cannot be trusted before correcting for the differences in the fiber-to-fiber response. This affects not only the comparison between adjacent spectra and the reconstructed 2D flux distributions, but it also strongly affects the sky-subtraction.

4.6 Flux calibration

Once the spectra are extracted, corrected for distortions, wavelength calibrated, and corrected for differences in transmission fiber-to-fiber, they must finally be flux calibrated. This calibration requires the observation of a spectrophotometric standard star during the night. As in slit-spectroscopy, where slit losses impose a severe limitation, absolute spectrophotometry with fiber-fed spectrographs is complex. Fiber-fed spectrographs suffer light losses when the fibers are smaller than the seeing-disc (or the astronomical target) and the calibration standard stars are not completely well centered in a single fiber. Both problems are better handled by IFUs, where the astronomical targets and the calibration stars are sampled by different fibers. However, IFUs based on pure fiber-bundles, like the PPAK mode of PMAS or INTEGRAL, do not cover the entire field-of-view (instead having typical fill-factors of $\sim 60\text{--}70\%$), which imposes flux losses. Other IFUs, like the PMAS/Larr or VIMOS, have solved this problem coupling a lensarray to the fiber-bundle. However, in most cases, it is not possible to obtain in a given night all the observations of spectrophotometric standards required to perform reliable absolute spectrophotometry. The most extended approach to solve the problem is to determine a relative spectrophotometry, and recalibrate the spectra later, using additional information, like broad-band photometry (e.g., García-Lorenzo et al. 2005, Sánchez et al. 2006b).

R3D includes a tool that compares the measured spectrum of a spectrophotometric standard star with the absolute values, convolving the spectra with a Gaussian kernel to degradate and match their resolutions. The ratio between both spectra at each wavelength, or the instrumental response, is stored and subsequently applied to the science frames to flux-calibrate them.

4.7 Sky Subtraction

The night sky emission spectrum must be subtracted from the science spectra. This subtraction should be performed before the flux calibration, if an external sky-frame is used, or can be done after it, if the sky is derived from the same dataset. In long-slit spectroscopy the sky is sampled in different regions of the slit (normally along the edges). In the most general case a median sky spectrum is obtained by averaging the spectra of these regions or interpolating (or extrapolating) them to the regions of the slit that sample the astronomical target. This is possible due to the size of the long-slits (typically several arcmins), compared with the size of the astronomical objects of interest. Unfortunately, the field-of-view of currently available IFUs is much smaller, being of the order of a few arcsecs to one arcmin (in the case of VIMOS or PPAK). If the astronomical objects fill all of the field-of-view, no spaxels sample any blank sky. In this case it is required to obtain supplementary sky exposures, and perform a direct subtraction of the reduced frames. On the other hand, if not all the field-of-view is filled with objects, it is possible to select those spectra free of contamination from objects, average them, and subtract it from the science spectra. This is simple to do using additional tools, such as E3D (Sánchez 2004).

Some spectrographs (e.g., PPAK, INTEGRAL) have designs that include additional fibers that probe the sky far enough from the science field-of-view to avoid contamination by the astronomical object. These *sky* fibers are normally distributed in between the science fibers across the entire pseudo-slit, in order to avoid any bias caused by the spectrograph off-axis position. R3D includes routines to extract and average the spectra obtained through these sky fibers, and subtract it from the science spectra.

As explained in section 3, imaging effects within the spectrograph and offsets at the fiber-slit change the effective dispersion, and have to be corrected by shifting, stretching, and interpolating the data to a linear wavelength coordinate system. However, this procedure does not correct for the differences in the shape of the emission lines along the cross-dispersion axis. This effect is also present in slit spectroscopy, and as a result, the sky-subtracted spectra show characteristic residuals in the location of the sky emission lines. The effect is more severe in fiber-based spectrographs, since the effective dispersion (and the shape of the emission lines) varies fiber-to-fiber. Therefore, even in the case of IFUs with *sky* fibers, an accurate decontamination from the sky emission is complex. R3D includes a specific tool for IFUs with *sky* fibers that determines the sky spectra corresponding to any science fiber by an interpolation of the spectra obtained through the *sky* ones. This tool increases the accuracy of the sky subtraction, compared with the results obtained by a simple averaging of the *sky* spectra. It takes into account the distortion in the wavelength solution along the cross-dispersion. However, it is still not optimal since it does not take into account the individual differences in the dispersion fiber-to-fiber. Figure 8 shows an exam-

ple of both sky subtraction procedures. More sophisticated procedures to subtract the sky have been performed in the data reduction techniques of different instruments (e.g., Bershadsky et al. 2005), but these are not currently implemented in R3D.

A more precise sky subtraction method is the nod & shuffle mode (e.g., Roth et al. 2005, Allington-Smith et al. 2002), that almost simultaneously records both sky and object spectra, using the identical optical path for both. While this method increases the accuracy of the sky subtraction, it doubles both the required exposure time, and the number of spectra at the CCD. R3D is also capable of reducing this type of data.

4.8 Re-ordering the spectra on the sky

As explained above, fiber-fed spectrographs and IFUs conduct light to the CCD from different positions in the sky. In both cases, but for IFUs in particular, it is important to re-order the spectra to their original positions in the sky. A position table is required, relating the spectra to their locations in the sky. Given this additional information, it is possible to use specific tools for IFS, like E3D (Sánchez 2004), to re-order the spectra. Then, it is possible to interpolate the data spatially and create a regular gridded datacube, and reconstruct the original image of the target at any wavelength, like the one shown in Fig. 7. Spatial interpolations are required in many cases, for example, to correct for differential atmospheric refraction (Sec. 4.9). This solution has been widely used in IFS, to become almost a standard procedure.

Some IFUs have lensarrays coupled to the fiber-bundles to avoid gaps in the coverage of the field-of-view (e.g., PMAS, VIMOS, GMOS). In some of them the lensarray already has a regular grid rectangular pattern (PMAS, VIMOS), while others have bee-cell-like hexagonal patterns (GMOS). In both cases spatial interpolation is not recommended in re-ordering the spectra to their locations in the sky. We included different procedures in R3D to reorder 2D RSS spectra of this kind of IFU into a datacube, following the pattern of their position table. The adopted solution is trivial for IFUs with regular grid rectangular lensarrays. This is not the case for lensarrays with hexagonal patterns.

The adopted solution in R3D for this latter kind of IFU is to create a regular grid rectangular datacube with the desired spatial pixel and covering the same wavelength range as the original 2D RSS frame. For each spatial pixel at each wavelength the recovered intensity would be the original one, if the pixel is included inside an hexagon cell, or an average of the intensities of the covered hexagons, if the pixel is in between different hexagon cells (weighted by the fraction of pixel area in each hexagon). Finally the obtained datacube must be corrected for differences in the input and output apertures (i.e., the ratio between the areas of the input and output spaxels). This solution, that we call *regularization*, does not impose any interpolation.

We used this *regularization* scheme to combine exposures taken at different adjacent positions in the sky with the

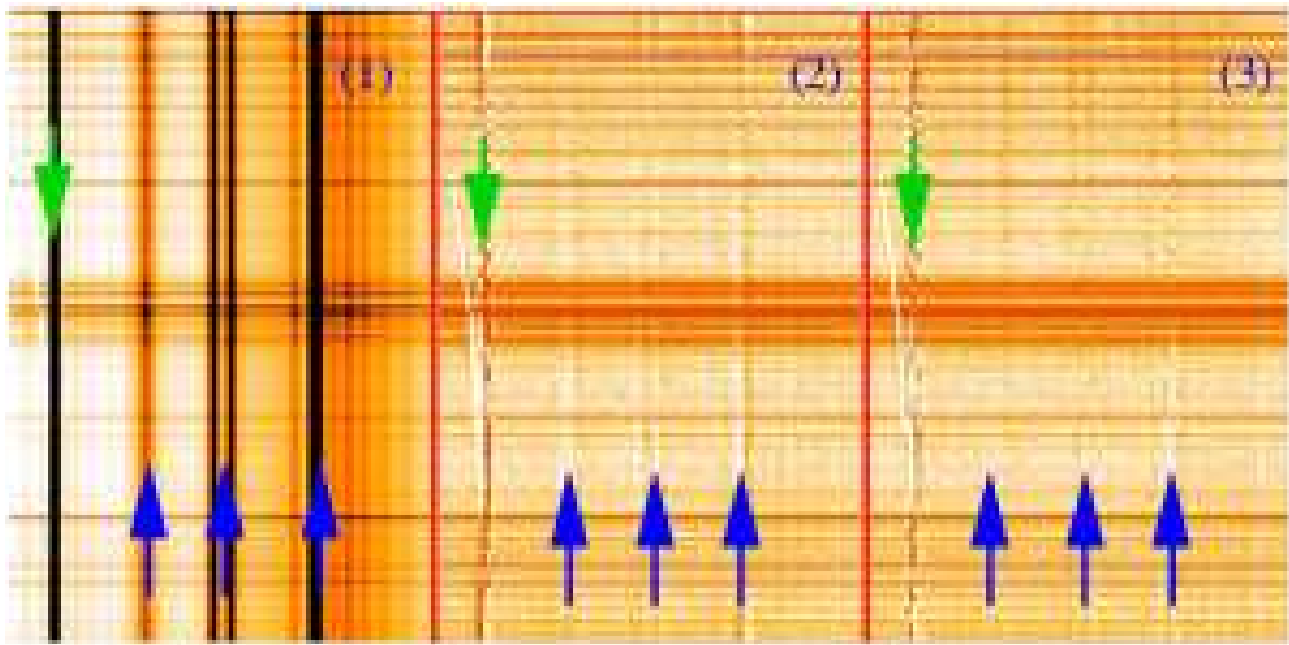


Fig. 8 Example of different methods for the sky subtraction. The left panel (1) shows reduced row-stacked spectra obtained with PMAS/PPAK. The central panel (2) shows the same exposure after subtraction of an average sky spectra. For the right panel (3) the sky spectrum was determined for each fiber by interpolating the sky spectra to the location of the science ones. Both images in panels (2) and (3) are plotted using the same grayscale. Arrows located at the top of the image indicate the sky-lines where the residuals are reduced, but still strong. Arrows located at the bottom of the image indicate the sky-lines where the residuals are clearly decreased.

same IFU (Mosaicing), with overlapping areas. It was also used to combine dithered exposures, obtained to cover the entire field-of-view using fiber-bundle IFUs (e.g., PPAK, Sánchez et al. 2006, Sánchez et al. 2006b). To our knowledge, the previous solution generally adopted was to interpolate each of the original pointings frames before combining. With that solution most of the combined intensities come from interpolated values, not from measured ones. With our adopted scheme, all the spectra result from the combination of measured values. On the other hand, the depth of the final datacube changes pixel-to-pixel in dithering schemes with low numbers of individual pointings.

4.9 Differential Atmospheric Refraction

IFS is capable of performing a correction of the differential atmospheric refraction (Filippenko 1982) after the observations, without requiring knowledge of the original orientation of the instrument and without the need of a compensator (Arribas et al. 1999, Roth et al. 2004). Reduced IFS data can be understood as a set of narrow-band images with a band-width equal to the spectral resolution. These images can be recentered using the theoretical offset determined by the DAR formulae (Filippenko 1982), or, as in 2D imaging, tracing the intensity peak of a reference object in the field-of-view (or a DAR reference observation) along the spectral range, and recentering it. Note that this latter approach is basically unfeasible in slit spectroscopy, this being one of the

fundamental differences between the two methods. The correction of the DAR is critical for the proper combination of different IFS exposures of the same object taken at different altitudes and under different atmospheric conditions. It is also fundamental for a proper alignment of mosaic and dither exposures.

R3D includes tools for tracing the location of the peak intensity of a particular object in the field-of-view along the dispersion axis. These locations are estimated by determining the centroid of the object in the image slice extracted at each wavelength from the datacube. Then, it is possible to shift the full datacube to a common reference by resampling and shifting each image slice at each wavelength (using an interpolation scheme), and storing the result in a new datacube. It is important to note here that any DAR correction imposes an interpolation in the spatial direction.

5 Comparison with other tools

Most of the techniques discussed in this article are well known by specialists, being implemented both in general packages like IRAF (Valdes 1992, Valdes 1992b), and in specific ones like PMAS (Becker 2001, Roth et al. 2005), the VIMOS (Scodreggio et al. 2005, Zanichelli et al. 2005) and GMOS reduction package (Turner et al. 2006). However, each implementation is somewhat different, affecting the reduction strategies and the results. It is unfeasible to compare our adopted implementations with those of all the

existing packages. Therefore, in order to illustrate them we compare briefly R3D and *dofibers*, a generalist tool for reducing fiber-fed spectroscopic data implemented in IRAF (Valdes 1992).

dofibers, like many other high-level tools in IRAF, compiles in a single task a series of different individual ones that are called (or not), in a sequential way. Each of these tasks corresponds, more or less, to each of the reduction steps explained through this article. As any other IRAF tool, it is possible to call it within a CL script, in a sequential way, as a single task or recursively. In all these aspects it seems remarkably similar to R3D. However, it has considerable differences.

As mentioned above, R3D is comprised of a set of sub-routines, each one related to a particular step of the data reduction. It is possible to modify any of the input parameters of each tool, storing the intermediate results. Any particular task at any step of the data reduction can be replaced with a similar one coded by the user and/or belonging to another reduction package. The intermediate results, like locating the spectra and tracing them, are amenable to simple modifications, making R3D a flexible tool. On the other hand, *dofibers* is a monolithic task, which does not allow full access to all the input parameters of the lower-level tasks called during the reduction process. Like any other IRAF tool, it relies on entries in certain header keywords. To replace a single task would require a deep knowledge of which headers modifies and the required output values. Furthermore, the output of the intermediate reduction steps are not stored in general and in many cases are difficult or impossible to modify (like the output of the tracing procedure).

Like in any other IRAF high-level tool, it is possible to use independently the different low-level tasks called by *dofibers*, creating your own high-level tool useful for a particular instrument (e.g., *doargus*, *dofoe*, *dohydra*...). These low level routines can be also modified, simplifying their use. For example, *int_apall*, the main task of the INTEGRAL reduction package (Arribas et al. 1998), is a simpler version of *apall* (one of the tasks called by *dofibers*), with most of the required parameters already pre-defined for each of the setups of this instrument.

5.1 Comparison step by step

Both R3D and *dofibers* require a pre-reduction of the raw data, that may include bias and dark correction, overscan trimming, and pixel-to-pixel flat-field correction. In *dofibers* this pre-reduction must be done with another IRAF tool, *ccdproc*. If not, the headers of the input files must be modified. In R3D, this pre-reduction can be performed with any external tool.

The *dofibers* procedure to locate the pixel of the intensity peak of each spectrum along the cross-dispersion axis is similar to that of R3D. However, the exact procedure to determine the centroid of those peaks differs. *dofibers* uses a sophisticated procedure included in *center1d*, which

relies on the contrast between the peak intensity and the supposed background. This procedure requires that the space in between fibers is large enough compared to the FWHM of the pseudo-Gaussian profiles to allow enough contrast of the peaks. As a result, it often fails to locate spectra in spectrographs with heavy fiber packing and strong cross-talk (e.g., MPSF, Becker 2001, Lehman et al. 2005). The solution adopted in R3D, a parabolic maximum determination, is less accurate, but more reliable in most cases. In addition, the difficulty to predefine or modify the estimated location of the spectra with *dofibers* makes it unfeasible for use in the reduction of data from spectrographs with many broken fibers and strong displacements of the location of the spectra frame-to-frame (e.g., VIMOS).

The tracing of peaks along the dispersion axis is also different. In *dofibers* this is performed every fixed number of pixels, and not in all of them (in general), as is done by R3D. After this non-contiguous search, the final trace is obtained by fitting the results with a polynomial function (Legendre, Chebyshev, or spline). The combination of a non-contiguous determination of the location of the spectra and the fitting of the results to a polynomial function, may produce significant deviations from the real trace if the input parameters are not handled with care.

The adopted solutions to determine and correct the scattered light are similar in both packages, with the difference being that in *dofibers* a 2D fitting is performed over the unmasked pixels (pixels not affected by signal from the spectra), while in R3D we perform a 1D fitting along the cross-dispersion axis for each pixel in the dispersion axis. In both packages the final result is smoothed before applying it.

The *dofibers* spectra extraction can be performed, as in R3D, by coadding the flux within a fixed aperture around the previously determined locations along the dispersion axis, also taking fractional pixels into account. *dofibers* also includes other extraction methods, such as variance weight flux extraction and adaptive apertures based on the contrast of intensity of the peaks (Valdes 1992b). On the other hand, it does not include any procedure to handle the cross-talk.

Distortion correction and derivation of the wavelength solution are performed in *dofibers* using the IRAF tools *identify*, *reidentify* and *dispcor*. These tools allow use of (i) comparison arcs taken immediately after each science frame, (ii) specific calibration spectra placed in between the science ones (e.g., as in PPAK, Kelz et al. 2006), and (iii) a series of arc frames that can be interpolated. In case (i) the procedure is remarkably similar to that adopted in R3D. However, with our adopted solution it is possible to use more emission lines than the identified ones to correct for the distortions of the spectra and resample them to the same wavelength solution. Case (ii) is strongly recommended not to be used, since the wavelength solution must be derived on a spectrum-by-spectrum basis. If not, it may produce substantial errors. Case (iii) may also be dangerous, since the interpolation of different arcs is based on their

distance in time with the science frame (defined by the julian date). In spectrographs that show strong flexures, like PMAS or VIMOS, this solution may produce strong deviations from the appropriate distortion correction and wavelength solution.

Another difference in this step lies in the adopted functions included in both packages to find the distortion correction and wavelength solution. Both *dofibers* and R3D include spline and Chebyshev functions. However, *dofibers* does not include linear polynomial functions, while R3D lacks Legendre polynomials. The adopted functions to interpolate and resample the spectra to a common linear wavelength solution are also different. While R3D only includes spline interpolations, *dofibers* includes three different interpolation functions.

The adopted schemes for correcting the differences in fiber-to-fiber transmission are similar in both packages, with the difference being in R3D it is possible to smooth the transmission ratio along the dispersion axis prior to applying it. In most cases this ratio has a smooth wavelength dependency, and a smoothing is recommended to increase the signal-to-noise. This solution is also included in other reduction tools, such as P3d (Becker 2001, Roth et al. 2005).

The sky subtraction scheme adopted in *dofibers* is the simpler method included in R3D, and consists of obtaining the median of the spectra marked as sky to create a single sky spectrum that is then subtracted from each spectrum in the dataset. This procedure, along with more refined improvements, have been discussed in previous sections.

Finally, it is important to note here that *dofibers* was designed to handle fiber-fed spectroscopic data but not IFS data. Therefore, it does not include any procedure to reorder the spectra in sky, correct for DAR, or perform 3D dithering or mosaicing.

6 Conclusions

This article has explained the particular characteristics of the raw data and data reduction of fiber-fed spectrographs in general and IFUs in particular. We presented a specialized package for reducing this kind of data, R3D, explaining in detail how the various steps in the data reduction process have been implemented. The effect of cross-talk and its possible solutions were discussed in detail, with simulations that illustrate them. R3D has been tested over several IFUs, including PMAS in its Lensarray and PPAK modes (which differs substantially), GMOS, VIMOS and INTEGRAL. Throughout this article we used PPAK data to illustrate how the data *evolve* after passing through each reduction step. The basic adopted solutions for the reduction steps were compared with those of the IRAF task *dofibers*, which is widely used to reduce this kind of data.

Integral Field Spectroscopy is evolving fast from a technique for specialists to a common user technique, and generalist tools, like R3D, are needed for the astronomical community. Thus we distribute the package freely. It provides a

common package for reducing data from any kind of fiber-fed spectrograph in general and IFUs in particular. We plan to extend it to other types of IFUs (such as TIGER-based lensarrays or Image Slicers). Use of R3D will help soften the learning curve for working with IFS data obtained with different IFUs.

Acknowledgements. We thank Dr. N. Cardiel for his invaluable help in the developing and testing process of R3D, and the polishing process of this article. We offered him to be co-author in this work, due to the amount of work that he did on it, although he kindly (and honestly) refused. He is always an inspiration of what an astronomer should be.

We thank Dr. M. Roth for his kindly help in cleaning the text of this article. We thank Dr. R. Gredel, director of Calar Alto, for supporting this work and providing me with the working and telescope time for finishing it. We thank the referee, Dr. A. Kelz, for the useful comments on the article. We also thank Dr. C.R. Benn and D. Coe who kindly revised the English style of this article, introducing valuable comments and corrections.

We thank support from the Spanish Plan Nacional de Astronomía program PNAyA2005, of the Spanish Ministry of Education and Science and the Plan Andaluz de Investigación of Junta de Andalucía as research group FQM322.

References

- Allington-Smith, J., et al. 2002, ASP Conf. Ser. 282: Galaxies: the Third Dimension, 282, 415
- Arribas S., Carter, D., Cavaller, L., et al.: 1998, Proc. SPIE, 3355, 821
- Arribas, S., Mediavilla, E., García-Lorenzo, B., del Burgo, C., & Fuensalida, J. J. 1999, A&AS, 136, 189
- Becker, T., Roth, M.M., Schmoll, J., 2000, ASP Conf. Ser. 195, p. 544
- Becker, T., 2001, PhD Thesis, Potsdam University
- Bershady, M. A., Andersen, D. R., Harker, J., Ramsey, L. W., & Verheijen, M. A. W. 2004, PASP, 116, 565
- Bershady, M. A., Andersen, D. R., Verheijen, M. A. W., Westfall, K. B., Crawford, S. M., & Swaters, R. A. 2005, ApJS, 156, 311
- Filippenko, A. V. 1982, PASP, 94, 715
- García-Lorenzo, B., Sánchez, S.F., Mediavilla, E., González-Serrano, J.I., Christensen, L., 2005, ApJ, 621, 146
- Jacoby, G. H., & Kaler, J. B. 1993, ApJ, 417, 209
- Kelz, A., Verheijen, M.A.W., Roth, M.M. et al., 2006, PASP, 118, 129
- Lehmann, I., et al. 2005, A&A, 431, 847
- LeFevre, O., Saisse, M., Mancini, D., et al. 2003, Proceedings of the SPIE, Volume 4841, pp. 1670-1681
- Meaburn, J., Blundell, B., Carling, R., Gregory, D. F., Keir, D., & Wynne, C. G. 1984, MNRAS, 210, 463
- Murray, G. J., Allington-Smith, J. R., Content, R., Dodsworth, G. N., Dunlop, C. N., Haynes, R., Sharples, R. M., & Webster, J. 2000, SPIE, 4008, 611
- Kissler-Patig, M., Copin, Y., Ferruit, P., Pécontal-Rousset, A., & Roth, M. M. 2004, AN, 325, 159
- Pearson, T.J., 1999, <http://www.astro.caltech.edu/~tjp/pgplot>
- Pécontal-Rousset, A., Copin, Y., & Ferruit, P. 2004, AN, 325, 163
- Roth, M. M., Becker, T., Kelz, A., & Schmoll, J. 2004, ApJ, 603, 531
- Roth, M.M., Kelz, A., Fechner, T., et al., 2005, PASP, 117, 620

- Sánchez, S. F. 2004, AN, 325, 167
- Sánchez, S. F., Cardiel, N., 2005, Calar Alto Newsletter, 10,
<http://www.caha.es/newsletter/news05b/Sanchez/index.html>
- Sánchez, S. F. Cardiel, N., Verheijen, M., Benitez, N., 2006,
Proceedings of “Sciences Perspectives for 3D Spectroscopy”,
ESO Astrophysics Symposia, Ed by M.Kissler-Patig, M.M.
Roth and J.R. Walsh (astro-ph/0512550)
- Sánchez, S. F. Cardiel, N., Verheijen, M., Covone, G., 2006, MN-
RAS, submitted.
- Scodeggio, M., et al. 2005, PASP , 117, 1284
- Turner, J. E. H., Miller, B. W., Beck, T. L., Song, I., Cooke, A. J.,
Seaman, R. L., & Valdés, F. G. 2006, New Astronomy Review,
49, 655
- Valdes, F. 1992, ASP Conf. Ser. 25: Astronomical Data Analysis
Software and Systems I, 25, 417
- Valdes, F. 1992, ASP Conf. Ser. 25: Astronomical Data Analysis
Software and Systems I, 25, 398
- Walsh, J. R. & Roth, M. M.: 2002, The Messenger, 109, 54
- Zanichelli, A., et al. 2005, PASP , 117, 1271